

OPTICAL TOMOGRAPHY

PACS numbers: 42.30.Wb; 42.25.Dd; 42.25.Fx
DOI: 10.1070/QE2014v044n03ABEH015342

Theoretical limit of spatial resolution in diffuse optical tomography using a perturbation model

A.B. Konovalov, V.V. Vlasov

Abstract. **We have assessed the limit of spatial resolution of time-domain diffuse optical tomography (DOT) based on a perturbation reconstruction model. From the viewpoint of the structure reconstruction accuracy, three different approaches to solving the inverse DOT problem are compared. The first approach involves reconstruction of diffuse tomograms from straight lines, the second – from average curvilinear trajectories of photons and the third – from total banana-shaped distributions of photon trajectories. In order to obtain estimates of resolution, we have derived analytical expressions for the point spread function and modulation transfer function, as well as have performed a numerical experiment on reconstruction of rectangular scattering objects with circular absorbing inhomogeneities. It is shown that in passing from reconstruction from straight lines to reconstruction using distributions of photon trajectories we can improve resolution by almost an order of magnitude and exceed the accuracy of reconstruction of multi-step algorithms used in DOT.**

Keywords: *spatial resolution, diffuse optical tomography, perturbation reconstruction model, point inhomogeneity, point spread function, modulation transfer function.*

1. Introduction

Modern nonlinear methods of diffuse optical tomography (DOT) [1–5], based on multi-step linearization of the problem of reconstruction and alignment at each step of the weight matrix, make it possible to produce images that are acceptable from the standpoint of the requirements to diagnosis of cancer. According to [6], the spatial resolution of diffuse tomograms is 4–6 mm inside an object 8–12 cm in size and 1–3 mm in the vicinity of its boundaries. Although these quantities are significantly inferior to resolution of X-ray computed tomography and magnetic resonance imaging, oncologists are quite happy with them because the contrast of diffusion tomograms visualising cancer is satisfactory for the correct diagnosis [7]. However, despite the rapid progress in computer technology, there are still no fast algorithms that implement nonlinear DOT methods, which would allow one to obtain images in real time. The time needed for diffusion tomograms to be reconstructed remains unacceptably long and amounts to tens of minutes and hours in 2D and 3D cases, respectively (see, for example, [2, 3, 8]). To this end, the researchers continue searching for a tradeoff between accuracy and speed of reconstruction, by developing more and more approximate methods that allow conventional formulation and (or) solving of the inverse problem of DOT. Among the approximate methods the most widely used are the so-called perturbation reconstruction methods [9–13], which neglect nonlinearity of the inverse DOT problem and reduce it to a linear Fredholm integral equation of the first kind. As a result, this approach makes it possible to restrict the consideration to single inversion of the system of linear algebraic equations describing the discrete model of reconstruction and to reduce the time of image reconstruction.

In this paper we study Lyubimov's perturbation reconstruction model [14, 15], which we adapted and developed in our previous studies [16–18] for the case of the time-domain technique of optical signal detection. According to this model, we should solve the following integral equation [17, 18]:

$$g(\boldsymbol{r}_\mathrm{s}, t_\mathrm{s}, \boldsymbol{r}_\mathrm{d}, t_\mathrm{d}) = \int_V [W_{\mu_\mathrm{a}}(\boldsymbol{r}_\mathrm{s}, t_\mathrm{s}, \boldsymbol{r}_\mathrm{d}, t_\mathrm{d}, \boldsymbol{r})\,\delta\mu_\mathrm{a}(\boldsymbol{r}) + W_D(\boldsymbol{r}_\mathrm{s}, t_\mathrm{s}, \boldsymbol{r}_\mathrm{d}, t_\mathrm{d}, \boldsymbol{r})\,\delta D(\boldsymbol{r})]\,\mathrm{d}^3 r, \quad (1)$$

where

$$W_{\mu_\mathrm{a}}(\boldsymbol{r}_\mathrm{s}, t_\mathrm{s}, \boldsymbol{r}_\mathrm{d}, t_\mathrm{d}, \boldsymbol{r}) = c\int_{t_\mathrm{s}}^{t_\mathrm{d}} P(\boldsymbol{r}, t\,|\,(\boldsymbol{r}_\mathrm{s}, t_\mathrm{s}) \to (\boldsymbol{r}_\mathrm{d}, t_\mathrm{d}))\,\mathrm{d}t, \quad (2)$$

$$W_D(\boldsymbol{r}_\mathrm{s}, t_\mathrm{s}, \boldsymbol{r}_\mathrm{d}, t_\mathrm{d}, \boldsymbol{r}) = -\frac{1}{D}\int_{t_\mathrm{s}}^{t_\mathrm{d}} P(\boldsymbol{r}, t\,|\,(\boldsymbol{r}_\mathrm{s}, t_\mathrm{s}) \to (\boldsymbol{r}_\mathrm{d}, t_\mathrm{d})) \times\Big[c\mu_\mathrm{a} + \frac{\partial}{\partial t}\ln G(\boldsymbol{r}-\boldsymbol{r}_\mathrm{s}, t-t_\mathrm{s})\Big]\mathrm{d}t. \quad (3)$$

Here, $(\boldsymbol{r}_\mathrm{s}, t_\mathrm{s})$ and $(\boldsymbol{r}_\mathrm{d}, t_\mathrm{d})$ are space-time points, which determine the position of the source and detector on the boundary of a scattering object of volume V; $g(\boldsymbol{r}_\mathrm{s}, t_\mathrm{s}, \boldsymbol{r}_\mathrm{d}, t_\mathrm{d})$ is the measurement result used directly for reconstruction; $W_{\mu_\mathrm{a}}(\boldsymbol{r}_\mathrm{s}, t_\mathrm{s}, \boldsymbol{r}_\mathrm{d}, t_\mathrm{d}, \boldsymbol{r})$ and $W_D(\boldsymbol{r}_\mathrm{s}, t_\mathrm{s}, \boldsymbol{r}_\mathrm{d}, t_\mathrm{d}, \boldsymbol{r})$ are the weighting functions, which take into account the contribution from each object point to the value of $g(\boldsymbol{r}_\mathrm{s}, t_\mathrm{s}, \boldsymbol{r}_\mathrm{d}, t_\mathrm{d})$; c, μ_a and D are, respectively, the speed, absorption and diffusion coefficients of light in the object; $\delta\mu_\mathrm{a}(\boldsymbol{r})$ and $\delta D(\boldsymbol{r})$ are the local spatial perturbations of optical parameters μ_a and D; $G(\boldsymbol{r}-\boldsymbol{r}', t-t')$ is Green's function of the unsteady diffusion equation; and $P(\boldsymbol{r}, t\,|\,(\boldsymbol{r}_\mathrm{s}, t_\mathrm{s}) \to (\boldsymbol{r}_\mathrm{d}, t_\mathrm{d}))$ is a function that has the meaning of the conditional probability density that a photon migrating from point $(\boldsymbol{r}_\mathrm{s}, t_\mathrm{s})$ to point $(\boldsymbol{r}_\mathrm{d}, t_\mathrm{d})$ at some intermediate instant of time t will reach the point $\boldsymbol{r} \in V$. According to [16], the relation

A.B. Konovalov, V.V. Vlasov Russian Federal Nuclear Center 'E.I. Zababakhin All-Russian Scientific Research Institute of Technical Physics', ul. Vasil'eva 13, 456770 Snezhinsk, Chelyabinsk region, Russia; email: a_konov@mail.vega-int.ru

Received 10 November 2013
Kvantovaya Elektronika **44** (3) 239–246 (2014)
Translated by I.A. Ulitkin

$$P(\boldsymbol{r},t\,|\,(\boldsymbol{r}_s,t_s)\rightarrow(\boldsymbol{r}_d,t_d))=\frac{G(\boldsymbol{r}-\boldsymbol{r}_s,t-t_s)\,G(\boldsymbol{r}_d-\boldsymbol{r},t_d-t)}{G(\boldsymbol{r}_d-\boldsymbol{r}_s,t_d-t_s)} \quad (4)$$

is valid for $P(\boldsymbol{r},t\,|\,(\boldsymbol{r}_s,t_s)\rightarrow(\boldsymbol{r}_d,t_d))$. The measurement result $g(\boldsymbol{r}_s,t_s,\boldsymbol{r}_d,t_d)$, we call time-resolved optical projection [17, 18], is given by

$$g(\boldsymbol{r}_s,t_s,\boldsymbol{r}_d,t_d)=-\ln\frac{\Gamma(\boldsymbol{r}_s,t_s,\boldsymbol{r}_d,t)|_{t=t_d}}{\Gamma_0(\boldsymbol{r}_s,t_s,\boldsymbol{r}_d,t)|_{t=t_d}}, \quad (5)$$

where $\Gamma(\boldsymbol{r}_s,t_s,\boldsymbol{r}_d,t)$ is the temporal point spread function (PSF) detected by a receiver at point $\boldsymbol{r}=\boldsymbol{r}_d$ from the source located at point $\boldsymbol{r}=\boldsymbol{r}_s$ in the case of the time-domain technique of data acquisition and the subscript '0' corresponds to a homogeneous scattering object not perturbed by the presence of optical inhomogeneities. The most important feature of model (1)–(3) is the fact that time-resolved optical projection (5) is found for only one time-gating delay t_d-t_s. This means that, in principle, for the image reconstruction it is necessary to know only one of the counts rather than the entire temporal PSF. This approach provides the best spatial resolution of the method by selecting the time-gating delay. In this paper, we focus on the accuracy of the reconstruction of diffusion tomograms rather that the speed of reconstruction. We demonstrate the possibility in principle to obtain with the help of model (1)–(3) the resolution, which is not inferior, but even higher than the resolution of exact multistep DOT algorithms. Regarding the speed of reconstruction, the computation time at this stage of research is not optimised, and the possibility of its reduction is discussed in Section 4.

Assessing the resolution limit, we compare the accuracy of three implementations of model (1)–(3): reconstruction from straight lines using the Radon inversion [19], reconstruction from the most likely trajectories of photons by using the method of average trajectories [16, 18, 20–24] and reconstruction based on the use of total banana-shaped distributions of photon trajectories [17]. The method of reconstruction from straight lines is based on the assumption of linearity and regularity of trajectories of signal propagation, which completely ignores the diffuse nature of photon migration in a scattering object and is therefore a very crude method of solving of the inverse DOT problem. The average trajectory method makes use of not straight lines but of photon average trajectories that bend near the boundaries of the scattering medium due to avalanche photon migration to outside the medium. Average trajectories quite correctly define the arrays of object points, the signals from which make the maximum contribution to the detected signal. The contributions from other points of the object are neglected. Only the reconstruction method using banana-shaped distributions of trajectories takes into account the contribution into the signal from each point of the object. For this reason, from the three listed methods, the third approach is the most appropriate method of reconstruction in terms of its compliance with an accurate model that is used to solve the forward DOT problem (radiative transfer equation, its diffusion approximation or the Monte Carlo method).

To estimate the resolution in the case of reconstruction from straight lines, we use analytical expressions for the PSF and the modulation transfer function (MTF), the derivation of which is given in Section 2. The assessment of resolution in the other two cases we obtain by analysing the results of the numerical experiment, within the framework of which we reconstruct rectangular scattering objects with circular absorbing inhomogeneities. In Section 3 we describe the numerical experiment, demonstrate and analyse the results obtained. In Section 4 we discuss and analyse the estimates of the resolution.

2. Theoretical approach to the assessment of resolution

To obtain the estimates of the limiting resolution, we use the approach developed for the case of X-ray tomography [25] and based on the approximation of a diffuse optical tomograph by a linear filter, which is invariant to the spatial shift. This approach involves the use of such characteristics as the PSF and MTF for the image quality assessment. Of course, in the general case any imaging system using diffuse scattered radiation is nonlinear and space-variant [26]. However, as shown by previous studies (see, for example, [6]), the model of a linear, space-invariant filter is convenient and useful for rough estimates of the characteristics of the image quality in localised areas of diffusion tomograms, where nonlinearity and spatial variance can be neglected in the first approximation. For example, to find the limiting resolution one should assess the image quality characteristics in the central region of the tomogram where blurring of reproducible spatial structures is maximal.

2.1. PSF on the optical projection

Consider the geometry of a flat layer for the 2D case (Fig. 1). Let $t_s=0$, the source be at point $\boldsymbol{r}_s(0,a)$, and the detector be at point $\boldsymbol{r}_d(l,-a)$. We pose the problem to calculate the time-resolved optical projection for a point absorbing inhomogeneity $\delta\mu_a(\boldsymbol{r})=\delta(x,y)$, located at the origin of the coordinates, as a function of distance l. According to (1) and (2) we have

$$g_\delta(l)=\int_S c\int_0^{t_d}P(\boldsymbol{r},t\,|\,(\boldsymbol{r}_s,0)\rightarrow(\boldsymbol{r}_d,t_d))\mathrm{d}t\;\delta(x,y)\mathrm{d}x\mathrm{d}y, \quad (6)$$

where S is the area of a scattering 2D object. In our previous works (see, for example, [16, 24, 27, 28]) we have shown that the standard root-mean-square deviation of photons from their average trajectory, which characterises the thickness of the light 'beam' in the scattering object and the actual image blurring, is weakly dependent on the geometry of the object. Under this assumption, we will use below simple analytical relations for infinite space. In the 2D case, we obtain an expression for infinite space

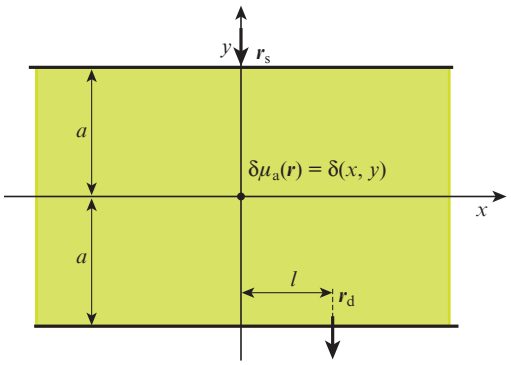

Figure 1. Data recording geometry.

$$G(\boldsymbol{r}-\boldsymbol{r}',t-t') = \frac{\exp[-\mu_a c(t-t')}{4\pi Dc(t-t')} \times\exp\left[-\frac{(x-x')^2+(y-y')^2}{4Dc(t-t')}\right], \quad (7)$$

$$P(\boldsymbol{r},t|\,(\boldsymbol{r}_s,0)\to(r_d,t_d)) = \frac{t_d}{4\pi Dct(t_d-t)} \times\exp\left\{-\frac{[xt_d-x_dt-x_s(t_d-t)]^2+[yt_d-y_dt-y_s(t_d-t)]^2}{4Dctt_d(t_d-t)}\right\}$$

$$= \frac{t_d}{4\pi Dct(t_d-t)}\exp\left\{-\frac{[xt_d-lt]^2+[yt_d-a(t_d-2t)]^2}{4Dctt_d(t_d-t)}\right\}. \quad (8)$$

Substituting (8) into (6) and integrating over the 2D space yield the one-fold integral:

$$g_\delta(l) = \frac{t_d}{4\pi D}\int_0^{t_d}\exp\left[-\frac{l^2t^2+a^2(t_d-2t)^2}{4Dctt_d(t_d-t)}\right]\frac{dt}{t(t_d-t)}, \quad (9)$$

which due to replacement $\alpha = t/(t_d-t)$ reduces to

$$g_\delta(l) = \frac{\exp[a^2/(2Dct_d)]}{4\pi D}\int_0^\infty\exp\left(-\frac{a^2+l^2}{4Dct_d}\alpha-\frac{a^2}{4Dct_d}\frac{1}{\alpha}\right)\frac{d\alpha}{\alpha}. \quad (10)$$

Using tables [29], we obtain

$$g_\delta(l) = \frac{\exp[a^2/(2Dct_d)]}{2\pi D}K_0\left(\frac{a\sqrt{a^2+l^2}}{2Dct_d}\right), \quad (11)$$

where $K_0(\xi)$ is the zero-order Macdonald function. Expression (11) is essentially a PSF on the optical projection $\mathrm{PSF}_{prj}(l)$, the final expression for which we obtain after normalisation by the condition

$$\int_{-\infty}^{\infty}\mathrm{PSF}_{prj}(l)\,dl = 1.$$

By setting

$$\mathrm{PSF}_{prj}(l) = AK_0\left(\frac{a\sqrt{a^2+l^2}}{2Dct_d}\right),$$

for the coefficient A we will have the expression [30]

$$A = \left[2\int_0^\infty K_0\left(\frac{a\sqrt{a^2+l^2}}{2Dct_d}\right)dl\right]^{-1}$$

$$= \left[2\int_a^\infty K_0\left(\frac{a\beta}{2Dct_d}\right)\frac{\beta d\beta}{\sqrt{\beta^2-a^2}}\right]^{-1} = \frac{a}{2\pi Dct_d}\exp\left(\frac{a^2}{2Dct_d}\right). \quad (12)$$

Thus, for the function $\mathrm{PSF}_{prj}(l)$ we obtain

$$\mathrm{PSF}_{prj}(l) = \frac{a\exp[a^2/(2Dct_d)]}{2\pi Dct_d}K_0\left(\frac{a\sqrt{a^2+l^2}}{2Dct_d}\right). \quad (13)$$

It is easy to see that at $a \geqslant 3\sqrt{Dct_d}$ use can be made of the asymptotic approximation of the Mcdonald function

$$K_n(\xi) \simeq \sqrt{\frac{\pi}{2\xi}}\exp(-\xi).$$

Then,

$$\mathrm{PSF}_{prj}(l) \simeq \left(\frac{a}{4\pi Dct_d\sqrt{a^2+l^2}}\right)^{1/2}\exp\left(\frac{a^2-a\sqrt{a^2+l^2}}{2Dct_d}\right). \quad (14)$$

Expression (14) is weakly dependent on the parameter a and is well approximated by a Gaussian function with a kernel $\sigma = \sqrt{2Dct_d}$:

$$\mathrm{PSF}_{prj}(l) \simeq \frac{1}{\sqrt{2\pi}\,\sigma}\exp\left(-\frac{l^2}{2\sigma^2}\right). \quad (15)$$

This result is in good agreement with Lyubimov's assessment [31] obtained for the instrumental function describing the image transfer through a flat layer of a scattering medium.

2.2. Assessment of resolution in the case of reconstruction from straight lines

The X-ray tomography experience suggests that in fact there are no stable algorithms that in the reconstruction process from straight lines make it possible to compensate for blurring of the structures obtained during projection. Local success, of course, can be achieved by applying, for example, a special projection filtering in the frequency domain [32, 33]. However, improving the spatial resolution, we risk obtaining a tomogram having artifacts that complicate the recognition of low-frequency structures [20, 21, 34]. Let us show by means of simple analytical calculations that in the case of DOT as well as in the case of X-ray tomography, we have very few chances to compensate for the projection blurring, if standard algorithms of reconstruction from straight lines are used.

Since the point inhomogeneity $\delta\mu_a(\boldsymbol{r}) = \delta(x,y)$ is axially symmetric, for the inverse projection of function (13), instead of the Radon inversion formulas, we can use one of the forms of the Abel inversion [19]:

$$\mathrm{PSF}_{bp}(r) = -\frac{1}{\pi r}\frac{d}{dr}\int_r^\infty\frac{\mathrm{PSF}_{prj}(l)\,l\,dl}{\sqrt{l^2-r^2}}$$

$$= -\frac{a\exp[a^2/(2Dct_d)]}{2\pi^2Dct_d}\frac{d}{rdr}\int_r^\infty K_0\left(\frac{a\sqrt{a^2+l^2}}{2Dct_d}\right)\frac{l\,dl}{\sqrt{l^2-r^2}}. \quad (16)$$

Performing consistently integration [30] and differentiation in (16), we obtain the expression for the PSF of the reconstructed image:

$$\mathrm{PSF}_{bp}(r) = \frac{a}{4\pi Dct_d\sqrt{a^2+r^2}}\exp\left(\frac{a^2-a\sqrt{a^2+r^2}}{2Dct_d}\right). \quad (17)$$

At $a \geqslant 3\sqrt{Dct_d}$ both PSF (17) and PSF (14) weakly depend on the parameter a and are well approximated by a Gaussian function with the kernel $\sigma = \sqrt{2Dct_d}$:

$$\mathrm{PSF}_{bp}(r) = \frac{1}{2\pi\sigma^2}\exp\left(-\frac{r^2}{2\sigma^2}\right). \quad (18)$$

Obviously, functions (18) and (15) coincide with the accuracy to the normalisation factor. Thus, after reconstruction from straight lines we have exactly the same blurring of the point inhomogeneity as it was on the projection.

To obtain an estimate of the MTF, it is necessary to apply the 2D Fourier transform to $\mathrm{PSF}_{bp}(r)$, which, as is known

[25, 35], in the case of axial symmetry is transformed into the Hankel transform. Thus, in the case of reconstruction from straight lines, the MTF has the form [30]

$$\begin{aligned}\mathrm{MTF}_{\mathrm{bp}}(\nu) &= \left| 2\pi \int_0^\infty \mathrm{PSF}_{\mathrm{bp}}(r) J_0(2\pi\nu r) r \mathrm{d}r \right| \\ &= \left| \frac{1}{\sigma^2} \int_0^\infty \exp\left(-\frac{r^2}{2\sigma^2}\right) J_0(2\pi\nu r) r \mathrm{d}r \right| \\ &= \frac{\pi^{3/2}\sigma\nu}{\sqrt{2}} \exp(-\pi^2\sigma^2\nu^2)[I_{-1/2}(\pi^2\sigma^2\nu^2) - I_{1/2}(\pi^2\sigma^2\nu^2)] \\ &= \exp(-2\pi^2\sigma^2\nu^2) = \exp(-4\pi^2 D c t_{\mathrm{d}} \nu^2), \end{aligned} \tag{19}$$

where ν is the radial spatial frequency; $J_0(\xi)$ is the zero-order Bessel function; and $I_n(\xi)$ is the nth-order modified Bessel function. Dependence (19) for the parameters c = 0.0214 cm ps^{-1}, D = 0.034 cm and t_{d} = 1000 ps is given in Fig. 2. The selected values of the optical parameters D and c are typical, for example, of breast tissue [18]. With regard to the time-gating delay of the detector, it is discussed in Section 4. Figure 2 shows that a 20% contrast (the Rayleigh conditional criterion of imaging resolution [35]) corresponds to a spatial frequency of 0.24 cycles cm^{-1} or a structure size of 2.1 cm. This result is significantly inferior to resolution estimates obtained in [6] and, of course, leaves much to be desired.

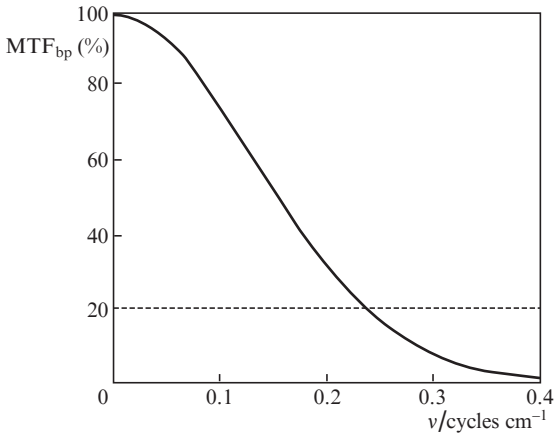

Figure 2. MTF for the case of reconstruction from straight lines.

3. Numerical experiment

3.1. Experimental setup

To evaluate the quality of diffusion tomograms by the method of photon average trajectories and banana-shaped distributions of trajectories, we carried out a numerical experiment, in which we used rectangular scattering objects 10 × 8 cm in size with circular absorbing inhomogeneities, simulated time-resolved optical projections, calculated average trajectories and banana-shaped distribution for different source–detector pairs and performed the appropriate reconstruction procedures. In total, we employed 32 sources and 32 detectors. Sources and detectors were located alternately and equidistantly on opposite sides of objects [faces $x = a$ and $x = -a$ (Fig. 1)]. Because we studied the 'transmission' regime, the couplings between sources and detectors located on one side of the object were ignored. Thus, the number of useful couplings used for reconstruction was equal to 32 × 16 (32 sources and 16 detectors). Calculations were performed for seven objects. Optical parameters of objects were as follows: c = 0.0214 cm ps^{-1}, D = 0.034 cm and μ_{a} = 0.05 cm^{-1}. To assess the PSF we considered an object containing a centrally located absorbing inhomogeneity 0.06 cm in diameter with an absorption coefficient μ_{a} = 0.5 cm^{-1}. To assess the MTF we used six objects, each of which comprised two circular absorbing inhomogeneities of the same diameter with the absorption coefficient μ_{a} = 0.075 cm^{-1}. Inhomogeneities were located near the centres of the objects and were separated from each other by a distance equal to their diameter. The diameters of the inhomogeneities of various objects varied from 1.2 to 0.2 cm with a step of 0.2 cm. To simulate time-resolved optical projections, we used the finite element method to solve the unsteady diffusion equation with an instantaneous point source. The temporal PSFs $\Gamma(\boldsymbol{r}_{\mathrm{s}}, t_{\mathrm{s}} = 0, \boldsymbol{r}_{\mathrm{d}}, t)$ for each source–detector pair were calculated as photon fluxes at the boundaries of objects in accordance with Fick's law [36]. Time-resolved optical projections were calculated by formula (5) for the delay time t_{d} = 1000 ps.

For the reconstruction of absorbing inhomogeneities, we used a discrete model in which the problem is reduced to solving a system of linear algebraic equations

$$\boldsymbol{g} = \hat{W}\boldsymbol{f}, \tag{20}$$

where $\boldsymbol{g} = \{g_i\}$ is the vector of time-resolved optical projections; $\boldsymbol{f} = \{f_i\}$ is the vector of discrete values of the reconstructed function; and $\hat{W} = \{W_{ij}\}$ is the matrix of weighting coefficients. When use is made of the method of average trajectories, the matrix of weighting coefficients is determined with the help of the approach described in detail in [18, 22–24]. For the reconstruction procedure to be regularised, instead of infinitely narrow average trajectories we used banana-shaped bands of finite width with vertices at points of location of sources and detectors. The formula for calculating the weighting coefficients has the form

$$W_{ij} = cS_{ij}/(v_{ij}d), \tag{21}$$

where S_{ij} is the area of the region of intersection of the ith banana-shaped band with the jth sampling cell in the reconstruction region; d is the linear cell size; and v_{ij} is the discrete value of the average rate of photon migration, for which the expression

$$v(t) = |\,\mathrm{d}\boldsymbol{R}(t)/\mathrm{d}t\,| \tag{22}$$

is valid, where the radius vector

$$\boldsymbol{R}(t) = \int_V \boldsymbol{r} P(\boldsymbol{r}, t\,|\,(\boldsymbol{r}_{\mathrm{s}}, 0) \to (\boldsymbol{r}_{\mathrm{d}}, t_{\mathrm{d}}))\,\mathrm{d}^3 r \tag{23}$$

describes the trajectory of the centre of mass of the distribution $P(\boldsymbol{r}, t\,|\,(\boldsymbol{r}_{\mathrm{s}}, 0) \to (\boldsymbol{r}_{\mathrm{d}}, t_{\mathrm{d}}))$, which in fact is the photon average trajectory. When banana-shaped distributions of trajectories are used for reconstruction, the matrix of weighting coefficients $\hat{W}$ is obtained by sampling the weight function $W_{\mu_{\mathrm{a}}}(\boldsymbol{r}_{\mathrm{s}}, t_{\mathrm{s}} = 0, \boldsymbol{r}_{\mathrm{d}}, t_{\mathrm{d}}, \boldsymbol{r})$, calculated for each source–detector pair in accordance with the approach outlined in [17]. This approach is based on the derivation of an exact analytical

expression for the function $P(\boldsymbol{r}, t\,|\,(\boldsymbol{r}_s, 0) \to (\boldsymbol{r}_d, t_d))$ in the half space, its numerical integration over time t and application of the method of centrally symmetric mapping in order to find the weighting function in the case of flat layer geometry.

In both cases, for the inversion of system (20), we used an iterative multiplicative algebraic reconstruction technique, modified by us to improve the convergence of the iterative process. The essence of the modification is that we take into account nonuniform distribution of sums of weighting coefficients in cells of the reconstruction region. The formula for the introduction of corrections to the solution on each $(s+1)$th iteration has the form [17, 18, 22–24]

$$f_j^{(s+1)} = f_j^{(s)} \left(\frac{g_i}{\sum_j W_{ij} f_j^{(s)}} \right)^{\lambda N W_{ij} / \sum_i W_{ij}}, \qquad (24)$$

where $\lambda \in (0, 1)$ is a parameter that controls the rate of convergence of the iterative process and N is the total number of source–detector couplings used for reconstruction. To ensure the maximal accuracy of reproduction of the structures, we reconstructed all seven objects on a very fine mesh (625×500) at a small control parameter ($\lambda = 0.05$). In this case, the regularised solution is reached after a few tens of iterations when use is made of the method of average trajectories and only after 5000–10000 iterations when use is made of distributions of trajectories.

3.2. Results of reconstruction and their analysis

Figures 3a and 3b show the results of reconstruction of the object for the PSF evaluation, obtained respectively using the method of average trajectories and banana-shaped distributions. Hereinafter, reconstruction results are presented as three-dimensional graphs $\delta\mu_a(x, y)$, and only the central part of the tomogram 5×4 cm in size being visualised. Figure 3c compares the amplitude-normalised profiles of the PSF obtained with the theoretical $\mathrm{PSF}_{bp}(r)$ [see equation (17)], which is also normalised in amplitude by the interval (0, 1]. One can clearly see that all PSFs have different full widths at half maximum. This indicates that unlike a crude model of reconstruction from straight lines, the models taking into account light propagation in an object allow one to minimise structure blurring obtained by projecting a point inhomogeneity. The smallest blurring and, hence, the maximum accuracy of structure reproduction are ensured by the method using banana-shaped distribution of photon trajectories.

Figure 4 shows the results of reconstruction of objects with two absorbing inhomogeneities. Left plots show tomograms reconstructed by the method of average trajectories, and right plots present the results of reconstruction using banana-shaped distributions. The diameter of the inhomogeneities is given in the upper right corner of each plot. It can be seen that the limiting resolution is close to 0.8 cm in the case of reconstruction by the method of average trajectories and is 0.2–0.4 cm in the case of reconstruction from the total distributions of photon trajectories. More accurate limiting resolution can be obtained if we construct the MTF. To do this, using the profile of each plot in Fig. 4 we estimate the modulation transfer coefficient as the relative depth of the dip between the two peaks. Discrete values of the spatial frequency are assigned to the diameter of the inhomogeneities. As the MTF, we consider the dependence of the modulation transfer coefficient on the spatial frequency (Fig. 5). One can

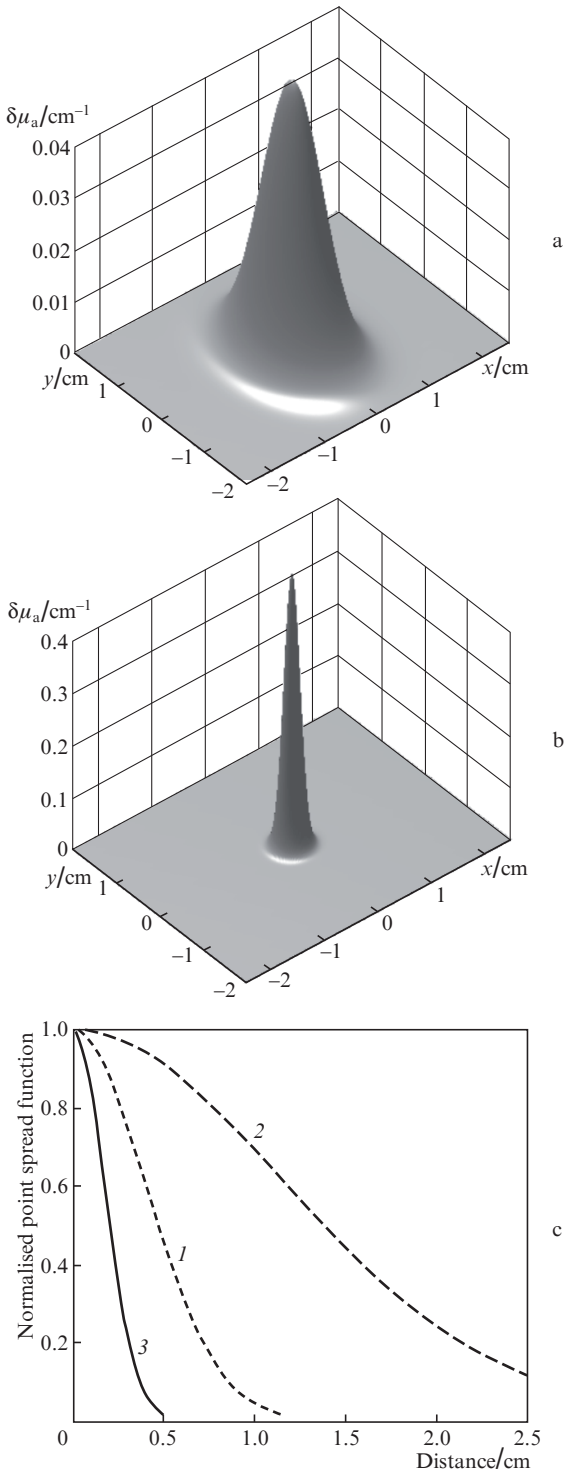

Figure 3. Results of reconstruction of the object for the PSF assessment by (a) the method of average trajectories and (b) banana-shaped distributions, as well as (c) normalised PSF profiles for the methods of average trajectories (*1*), straight lines (*2*) and banana-shaped distributions (*3*).

see from Fig. 5 that structures with frequencies of no more than 0.7 and 2.2 cycles cm^{-1} (i.e., the size of at least 0.72 and 0.23 cm) will be reconstructed with the contrast of at least 20% by using the method of average trajectories and the total banana-shaped distributions, respectively. The latter figure is undoubtedly noteworthy because it characterises the resolution exceeding that of exact multistep DOT algorithms.

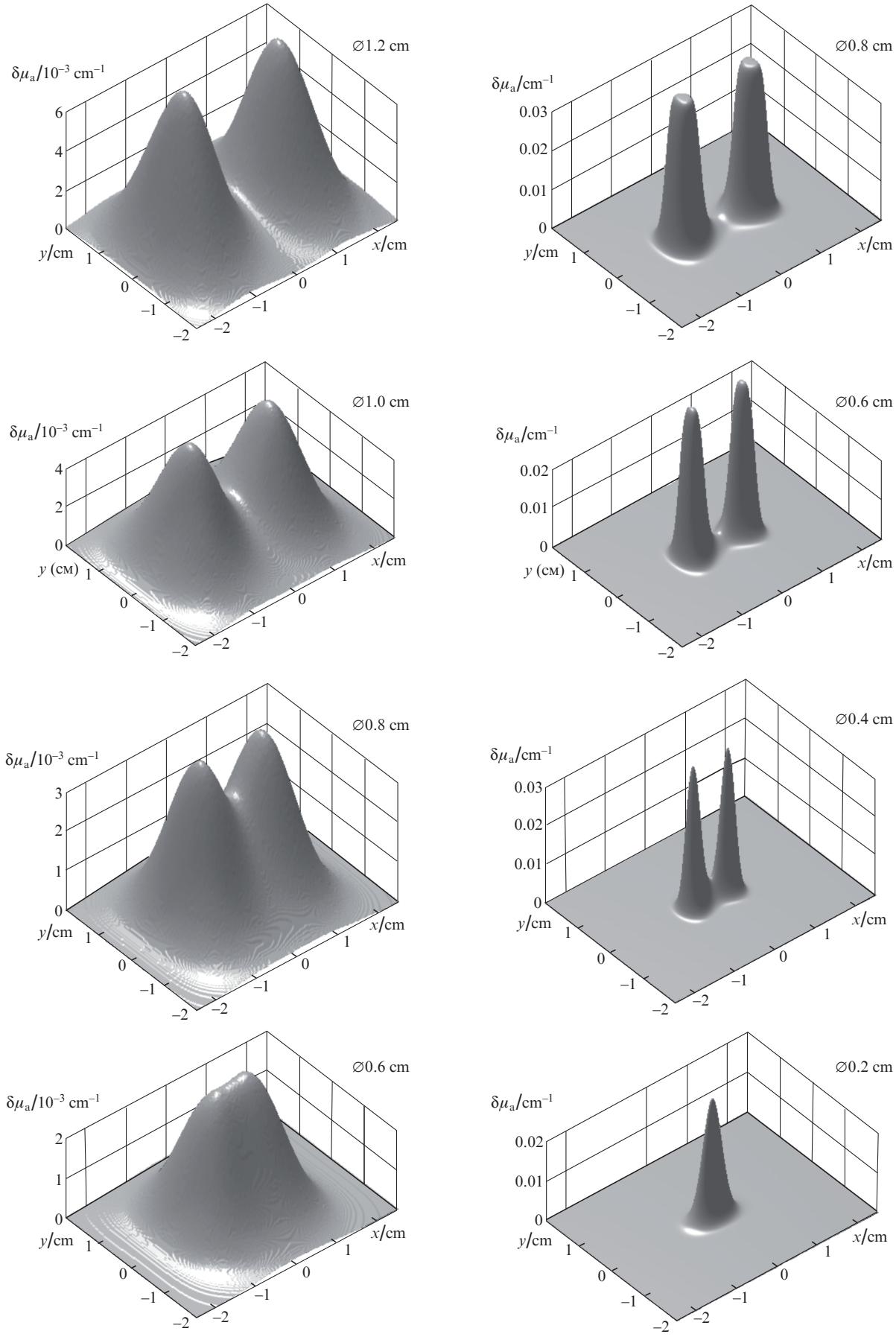

Figure 4. Results of reconstruction of objects with two absorbing inhomogeneities.

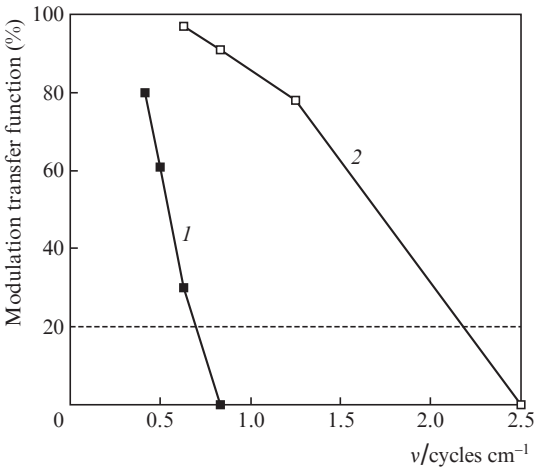

Figure 5. MTF for cases of reconstruction from (*1*) average trajectories and (*2*) banana-shaped distributions.

4. Discussion of the results

In papers [14, 31, 37] Lyubimov hypothesised that the spatial resolution of time-domain DOT can be estimated as the root-mean-square deviation of photons from their average trajectory, which characterises the width of the banana-shaped distribution of photon trajectories. In the case of the perturbation model (1)–(3), for the root-mean-square deviation we have the expression [14, 16, 18, 20–24, 27, 28, 37]

$$\Delta(t) = \left[\int_V |\boldsymbol{r} - \boldsymbol{R}(t)|^2 P(\boldsymbol{r}, t \,|\, (\boldsymbol{r}_s, t_s) \;\rightarrow\; (r_d, t_d))\, \mathrm{d}^3 r\right]^{1/2}. \quad (25)$$

Statistical characteristics of the distributions of photons, including the second moment $\Delta(t)$, we investigated for different geometries of the scattering object in a number of studies [16, 18, 24, 27, 28, 37]. We proved that $\Delta(t)$ is weakly dependent on the geometry of the object. This especially holds true in the central region, which is the remotest from the object boundaries, where the root-mean-square deviation takes maximum values. Using (8), (23) and (25) it is easy to show that in the case of an infinite 2D space, the relation

$$\Delta(t) = \left[\frac{4Dct(t_d - t)}{t_d}\right]^{1/2} \quad (26)$$

is valid. The maximum of function (26) is reached at $t = t_d/2$:

$$\Delta_{max} = \Delta(t_d/2) = \sqrt{Dct_d}\,. \quad (27)$$

By substituting the values of the optical parameters and t_d selected in Section 2 into (27), we obtain $\Delta_{max} \simeq 0.85$ cm. Comparing this value with the resolution estimates obtained in Sections 2 and 3, we see that the root-mean-square deviation of photons from their average trajectories can indeed serve a measure of spatial resolution in DOT using a perturbation model. For the limiting resolution Δr_{lim} we can write the expression:

$$\Delta r_{lim} = \gamma \Delta_{max}. \quad (28)$$

In this case, the coefficient of proportionality γ is close to 0.9 in the case of reconstruction from average trajectories, is equal to ~2.5 in the case of reconstruction from straight lines and is close to 0.3 in the case of reconstruction of tomograms from banana-shaped distribution of photon trajectories.

It should be noted that the excellent results obtained in the latter case are largely due to the unique ability to use for reconstruction the time-resolved optical projections [model (1)–(3)], which are found for a single time-gating delay of the detector. Multistep algorithms of time-domain DOT do not have this capability, because they use for reconstruction the integrated data, such as integrated intensity, average time of flight of photons, results of the Mellin–Laplace transform of the temporal PSF, etc. (see, for example, [1]). The selection of time delay (1000 ps) is caused by the desire to minimise the blurring of inhomogeneities and, hence, the spatial resolution. It is clear that, in accordance with formulas (27) and (28) we are interested in selecting the smallest value of time delay. On the other hand, this value should provide a signal-to-noise ratio acceptable for qualitative reconstruction of tomograms. According to studies [18], the minimum time delay satisfying this requirement for a given geometry is close to 1000 ps. However, despite the fact that we reasonably selected the time delay based on practical grounds, noise in this paper was not modelled and we used 'ideal' (noiseless) data for reconstruction. Therefore, the quantitative assessment obtained should be considered as the estimate of the theoretical resolution limit. This means that in a real physical experiment somewhat less optimistic results can be obtained.

It was noted above that the computation rate was not optimised at this stage of the research. In the case of banana-shaped distributions, the time needed to reconstruct a single image on an Intel PC (1.7-GHz Pentium 4, 512-MB RAM) in MATLAB is a few hours. According to our estimates, by selecting the optimal size of the mesh and the control parameter λ, as well as by optimising the code and using a software environment faster than MATLAB, the computation rate can be increased by several times. Of particular interest is the application of an object-oriented programming to the implementation of our iterative algorithm on graphics processing units. In this case, as the experience of our colleagues [38] shows, the gain in the computation rate can achieve two or more orders of magnitude.

5. Conclusions

In this paper we have estimated the theoretical limit of spatial resolution of time-domain DOT based on a perturbation model. It is shown that this model using for reconstruction the time-resolved optical projections allows one, in principle, to obtain the spatial resolution, which is not inferior to resolution of exact multistep DOT algorithms and even exceeds it. In order to adequately compensate for the structure blurring obtained by registering a diffusely scattered signal, the reconstruction process must be based on total banana-shaped distributions of photon trajectories, which make it possible to take into account the contribution from each object point into the recorded signal. Banana-shaped distributions are calculated semi-analytically using diffusion approximations of the radiative transfer equation.

We can expect that by optimising the computation time, the DOT method considered in this paper can prove competitive and called for in practice, for example, in optical mammography for reconstruction of functional parameters of mammary gland.

Acknowledgements. The authors are grateful to V.V. Lyubimov without whose theoretical studies (see, for example, [14, 15, 31, 37]) the publication of this paper would have been impossible.

References

1. Arridge S.R. *Inverse Prob.*, **15**, R41 (1999).
2. Hielscher A.H., Klose A.D., Hanson K.M. *IEEE Trans. Med. Imaging*, **18**, 262 (1999).
3. Schweiger M., Arridge S.R., Nissilä I. *Phys. Med. Biol.*, **50**, 2365 (2005).
4. Dehghani H., Eames M.E., Yalavarthy P.K., Davis S.C., Sriniva-san S., Carpenter C.M., Pogue B.W., Paulsen K.D. *Commun. Numer. Methods Eng.*, **25**, 711 (2008).
5. Arridge S.R., Schotland J.C. *Inverse Prob.*, **25**, 123010 (2009).
6. Pogue B.W., Davis S.C., Song X., Brooksby B.A., Dehghani H., Paulsen K.D. *J. Biomed. Opt.*, **11**, 033001 (2006).
7. O'Sullivan T.D., Cerussi A.E., Cuccia D.J., Tromberg B.J. *J. Biomed. Opt.*, **17**, 071311 (2012).
8. Enfield L.C., Gibson A.P., Everdell N.L., Delpy D.T., Schweiger M., Arridge S.R., Richardson C., Keshtgar M., Douek M., Hebden J.C. *Appl. Opt.*, **46**, 3628 (2007).
9. Kak A.C., Slaney M. *Principles of Computerized Tomographic Imaging* (New York: IEEE Press, 1988).
10. Feng S., Zeng Z.-A., Chance B. *Appl. Opt.*, **34**, 3826 (1995).
11. Arridge S.R. *Appl. Opt.*, **34**, 7395 (1995).
12. Markel V.A., Schotland J.C. *J. Opt. Soc. Am. A*, **18**, 1336 (2001).
13. Markel V.A., Schotland J.C. *Phys. Rev. E*, **70**, 056616 (2004).
14. Lyubimov V.V. *Opt. Spektrosk.*, **80**, 687 (1996).
15. Kravtsenyuk O.V., Lyubimov V.V. *Opt. Spektrosk.*, **89**, 119 (2000).
16. Lyubimov V.V., Kalintsev A.G., Konovalov A.B., Lyamtsev O.V., Kravtsenyuk O.V., Murzin A.G., Golubkina O.V., Mordvinov G.B., Soms L.N., Yavorskaya L.M. *Phys. Med. Biol.*, **47**, 2109 (2002).
17. Konovalov A.B., Vlasov V.V., Uglov A.S., Lyubimov V.V. *Proc. SPIE Int. Soc. Opt. Eng.*, **8088**, 80880T (2011).
18. Konovalov A.B. *Cand. Diss.* (Snezhinsk, Russian Federal Nuclear Center – VNIITF, 2012).
19. Pikalov V.V., Preobrazhenskii N.G. *Vychislitel'naya tomografiya v gazovoi dinamike i fizike* (Reconstruction Tomography in Gas Dynamics and Plasma Physics) (Novosibirsk: Nauka Sib. Otd., 1987).
20. Konovalov A.B., Lyubimov V.V., Kutuzov I.I., Kravtsenyuk O.V., Murzin A.G., Mordvinov G.B., Soms L.N., Yavorskaya L.M. *J. Electron. Imaging*, **12**, 602 (2003).
21. Lyubimov V.V., Konovalov A.B., Kutuzov I.I., Kravtsenyuk O.V., Kalintsev A.G., Murzin A.G., Golubkina O.V., Soms L.N., Yavorskaya L.M. *Opt. Zh.*, **70** (10), 37 (2003).
22. Konovalov A.B., Vlasov V.V., Kalintsev A.G., Kravtsenyuk O.V., Lyubimov V.V. *Kvantovaya Elektron.*, **36**, 1048 (2006) [*Quantum Electronics*, **36**, 1048 (2006)].
23. Konovalov A.B., Vlasov V.V., Mogilenskikh D.V., Kravtsenyuk O.V., Lyubimov V.V. *Kvantovaya Elektron.*, **38**, 588 (2008) [*Quantum Electronics*, **38**, 588 (2008)].
24. Konovalov A.B., Vlasov V.V., Lyubimov V.V. *Optik*, **124**, 6000 (2013).
25. Konovalov A.B., Vlasov V.V. *ISRN Sign. Process.*, **2013**, 356291 (2013).
26. Konovalov A.B., Vlasov V.V., Kravtsenyuk O.V., Lyubimov V.V. *EURASIP J. Adv. Sign. Process.*, **2007**, 34747 (2007).
27. Volkonskii V.B., Kravtsenyuk O.V., Lyubimov V.V., Mironov E.P., Murzin A.G. *Opt. Spektrosk.*, **86**, 299 (1999).
28. Kravtsenyuk O.V., Lyubimov V.V. *Opt. Spektrosk.*, **88**, 670 (2000).
29. Prudnikov A.P., Brychkov Yu.A., Marichev O.I. *Integrals and Series, Vol. 1: Elementary Functions* (New York: Gordon and Breach, 1986).
30. Prudnikov A.P., Brychkov Yu.A., Marichev O.I. *Integrals and Series, Vol. 2: Special Functions* (New York: Gordon and Breach, 1990).
31. Lyubimov V.V. *Opt. Spektrosk.*, **76**, 725 (1994).
32. Vainberg E.I., Kazak I.A., Kurozaev V.P. *Dokl. Akad. Nauk SSSR*, **257**, 89 (1981).
33. Gonzalez R.C., Woods R.E. *Digital Image Processing* (New Jersey: Prentice Hall, 2002).
34. Kalintsev A.G., Kalintseva N.A., Kravtsenyuk O.V., Lyubimov V.V. *Opt. Spektrosk.*, **99**, 162 (2005).
35. Papoulis A. *Systems and Transforms with Applications in Optics* (New York: McGraw-Hill, 1968).
36. Duderstadt J.J., Hamilton L.J. *Nuclear Reactor Analysis* (New York: Wiley, 1976).
37. Lyubimov V.V. *Opt. Spektrosk.*, **86**, 297 (1999).
38. Doronin A., Meglinski I. *Biomed. Opt. Express*, **2**, 2461 (2011).